Progress In Electromagnetics Research M, Vol. 11, 1–12, 2010

GAUSSIAN BEAM MODELING OF SAR ENHANCEMENT IN PARAXIAL AND NON-PARAXIAL REGIONS OF BIOLOGICAL TISSUES

M. L. D. Lumori

Department of Engineering
University of San Diego
5998 Alcala Park, San Diego, CA 92110, USA

Abstract—A polarized 3D-electromagnetic wave propagating from an aperture source into a lossy medium can be modeled by an astigmatic Gaussian beam model (GBM) of complex source coefficients that characterize a radiating antenna uniquely. The source coefficients are determined numerically from phantom experiments, and then used in simulations of specific absorption rates (SAR), in both homogeneous and layered biological media, resulting in good agreement with experimental data. This paper shows that for an x-polarized E-field the GBM simulations of SAR enhancement or focus in the axial, z-directed, paraxial region are accurate, but approximate in the transverse, y-directed, non-paraxial regions due to a focal shift.

1. INTRODUCTION

The Gaussian beam model (GBM) was developed for application to electromagnetic hyperthermia and treatment planning of superficial tumors, such as breast cancer. Its attributes include the following [1–7]:

- In a treatment planning setup, a water-bolus is placed between the aperture antenna (applicator) and the body (muscle and/or lung phantom) for matching and cooling. The entire system is modeled by the GBM using electric field measurements from a liquid muscle-like phantom. Any other model which precludes the fields in the aperture–bolus–air–phantom interfaces is apt to err [2–4].
- Simplicity of application (a few seconds of CPU real time) to treatment planning of superficial tumors for both single-element

Corresponding author: M. L. D. Lumori (mlumori@sandiego.edu).

and multi-element phased arrays applied to homogeneous and layered media [4].

- Flexibility in modeling positional shifts, orientation, amplitude variations, inter-element spacing for optimal SAR (specific absorption rates), inter-element field coupling, and SAR focusing at tumor targets [2, 4, 5].
- Simulation and modeling of coherent SAR (for deep, narrow chest-wall lesions) and incoherent SAR (for shallow, wide chest-wall lesions) [7].

The development of the Gaussian beam model for hyperthermia application was based on propagation of electromagnetic waves as a bundle of complex rays [8, 9] which hug the paraxial regions. To this end, this paper addresses the extent to which the GBM-simulated enhancement (focal) results differ from the expected results. It has been proven experimentally that the GBM is accurate and has focusing capabilities in lossy media, contrary to established theory pertaining to Gaussian beams in free space [10–12]. This is because the limitations imposed by free space do not exist in lossy media, where the high spatial frequencies are damped out, leaving a smooth distribution which can be verified experimentally [2–4]. Furthermore, it has been demonstrated in [2] that the GBM is the exact solution to the *parabolic partial differential equation* — PPDE (or Schrödinger-type equation), discussed in Section 2 and illustrated schematically in Fig. 1. Some of the published literature on GBM-simulated results is available for the SMA Co. horn antenna [3, 4, 13] and for the current sheet applicator (CSA) [5, 14, 15], both shown in Fig. 2. In addition to homogeneous media, the GBM has been developed to model up to 3-layered media [2, 4, 5].

The thrust of this paper pertains to SAR enhancement in homogeneous media with a special emphasis on focal errors when current sheet applicators (CSA) are used to target tumor sites. The presented results can be replicated in layered media and for other applicator types used for treatment planning in cancer therapy.

2. FUNDAMENTAL GBM THEORY AND WAVE-FRONTS

Consider the scalar wave equation:

$$\left(\nabla^2 + k^2\right) U(x, y, z) = 0 \tag{1}$$

Assuming that energy flow is predominantly in the z-direction, we pull out the dominant axial term from (1), *viz*:

$$U(x, y, z) = \psi(x, y, z) e^{-jkz} \tag{2}$$

The differential equation for $\psi(x, y, z)$ in (2), a slowly varying function, is

$$\frac{\partial^2\psi}{\partial x^2} + \frac{\partial^2\psi}{\partial y^2} - 2jk\frac{\partial\psi}{\partial z} + \frac{\partial^2\psi}{\partial z^2} = 0 \tag{3}$$

where $k = \omega\sqrt{\mu\varepsilon}(1 - j\frac{\sigma}{\omega\varepsilon})^{1/2}$ is a complex propagation constant, with σ the conductivity, $\varepsilon = \varepsilon_0\varepsilon_r$ the permittivity and $\mu = \mu_0$ the permeability of the medium, and ω the angular frequency of the wave. Invoking the high-frequency asymptotic approximation where the second-order axial derivative $\frac{\partial^2\psi}{\partial z^2}$ is negligible, leads to the PPDE. The propagation constant k is related to its axial and transverse components, *viz*:

$$k^2 = k_x^2 + k_y^2 + k_z^2 \tag{4}$$

Define the square of the transverse wave number as $k_t^2 = k_x^2 + k_y^2$, where for a z-directed, paraxial beam:

$$k_z^2 \gg k_t^2 \quad \text{with} \quad k_t \ll k \tag{5}$$

From (4) and (5), it can be shown that:

$$k_z \cong k - \frac{1}{2}\frac{k_t^2}{k} \quad \text{or, by (5)} \quad k_z \cong k \tag{6}$$

The approximation leading to Equation (6) results in the PPDE [2], whose solution is the following astigmatic beam expression [12], which is the GBM:

$$E(x, y, z) = \frac{E_0 e^{-jkz}}{\sqrt{(z-a)(z-b)}} \times e^{-j\frac{kx^2}{2(z-a)}} \times e^{-j\frac{ky^2}{2(z-b)}} \tag{7}$$

where a and b are complex source coefficients that characterize an applicator uniquely, and E_0 is an arbitrary real constant. The dimensions of a and b, their geometrical determination, and their corresponding effects on the wave-fronts as well as their influence on the transverse and axial decays of the E-field are discussed in [1, 2, 4]. An accurate, experimentally-based numerical method (OPT_GBM) for determining a and b is reported in [3]; it is an improvement on the geometrical method (GEO_GBM) presented in [4].

In (6) and Fig. 1, the reciprocals of the wave numbers are distances from the point source; they correspond to the curvature and propagation of the wave fronts emanating from the point source.

As illustrated in Fig. 1, $1/k$ traces out a circle everywhere (sphere in 3D). On the other hand, $1/k_z$ traces out a circle in the paraxial (axial, z-directed) region (sphere in 3D), and it traces out a parabola (paraboloid in 3D) in the non-paraxial regions. This implies that the GBM predicts accurate SAR in the paraxial region, but approximate

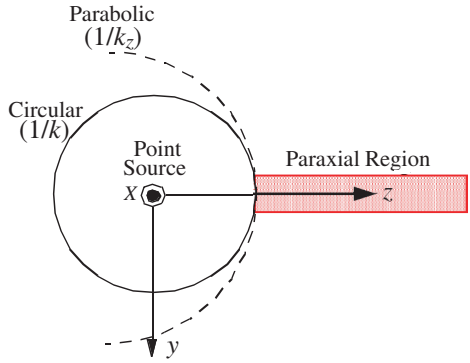

Figure 1. Paraxial and non-paraxial wave fronts ($1/k$ and $1/k_z$) of an x-polarized E-field, $E_x(y, z)$.

SAR in the non-paraxial region. Hence, an antenna can be designed such that it radiates maximum electromagnetic fields in the axial, z-direction with its aperture restricted, approximately, to the paraxial region in Fig. 1.

Next, we determine SAR enhancement (focus) via an analytical formulation, based on [2, 16, 17]: Consider an array of N-element applicators driven coherently [2, 4, 5, 7] to achieve focus at a tumor site. From (7), for an x-polarized electric field $E_x(y, z)$, the field contribution due to the nth element ($n = 1, 2, 3, \ldots, N$) is of the form:

$$E_{x,n}(y, z) = \Delta_n e^{j\delta_n} \times |E_x(y, z)| \times e^{j\phi_n(y,z)} \tag{8}$$

In (8), Δ_n and $\phi_n(y, z)$ are the respective relative amplitude and phase of the field for the nth element, with δ_n the corresponding phase required for focus, defined below, in (9). The value of Δ_n is set as desired and focusing at the focal point (y_{focus}, z_{focus}) is dictated by the following expression:

$$\delta_n = -\phi_n(y_{focus}, z_{focus}) \tag{9}$$

The total electric field distribution is

$$E_T(y, z) = \sum_{n-0}^{N-1} E_{x,n}(y, z) \tag{10}$$

The focused power distribution in a homogeneous medium of conductivity σ-S m^{-1} is given by:

$$P_F(y, z) = \frac{1}{2}\sigma \, |E_T(y, z)|^2 \ \text{W/m}^3 \tag{11}$$

Hence, the focused relative power distribution or enhanced SAR is

$$P_{Rel} = \frac{P_F(y,z)}{P_{\max}(y,z)} \tag{12}$$

3. MATERIALS AND EXPERIMENTAL METHOD

A liquid muscle-like phantom was used in the experiment [2, 4, 5]. The conductivity and relative permittivity of the phantom varied with frequency, saline concentration, and temperature [18]. A non-rectifying electric field probe was required to scan the field in the phantom. Oriented parallel to the dominant linearly polarized electric field (x-polarized), the probe consisted of a balanced dipole 10 mm long, 5 mm wide, formed by stripping a semi-rigid micro-coaxial cable 1.5 mm in diameter [6]. Fig. 2 depicts the SMA (driven at 400 MHz) and CSA (driven at 450 MHz) applicators; also their measured phases and relative amplitudes are shown in Fig. 3.

The spatial distributions of the electric field were determined in the principal E- and H-planes of the CSA, close (1.0 cm) to the aperture by scanning the field probe in the liquid phantom under computer control [3–5]. The measurements were processed in a network analyzer (Hewlett Packard Model 8754A) for phase, relative electric

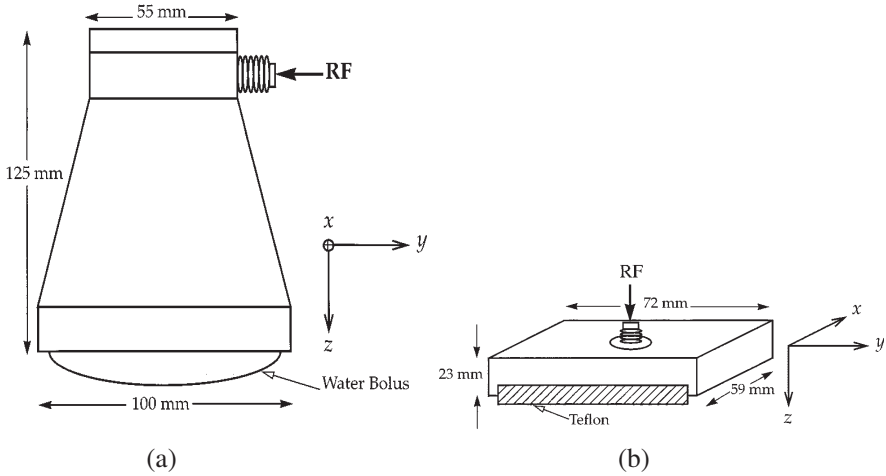

Figure 2. Schematics of (a) SMA (Italian Company) multifrequency water-loaded waveguide applicator with a circular aperture [4, 13] and (b) current sheet applicator (CSA): Inductive microwave aperture antenna with a Teflon aperture for interface matching [5].

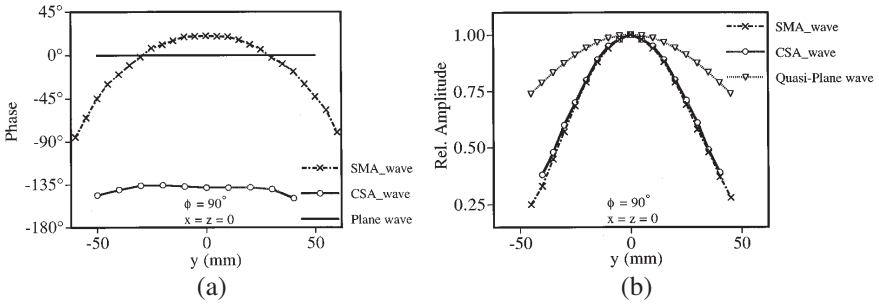

Figure 3. Principal E-plane experimental (SMA_wave & CSA_wave) and theoretical (plane- and quasi-plane-waves) results of (a) field phase and (b) relative field amplitude, close ($z = 1.0\,\text{cm}$) to the apertures.

field amplitude and power data. Thus, the source parameters of both applicators were determined experimentally via the geometrical method (GEO_GBM) [3–5] to be

- CSA: $a = -3.6492 - j9.3903\,\text{cm}$ and $b = -0.4140 - j6.6189\,\text{cm}$ (13)
- SMA: $a = -2.7066 - j3.6810\,\text{cm}$ and $b = -3.7391 - j4.6112\,\text{cm}$ (14)

The parametric values in (13) and (14) are unique characteristics of the applicator type; they are complex source points from which electromagnetic waves emanate [2, 4, 5]. Hence, using these values in Equations (7)–(12) it is possible to determine focused power distributions (SAR) in a biological target, such as a lung tumor, as demonstrated in the next section. The following observations are worth noting:

- The experimental procedure used in conjunction with the GBM to determine the source parameters in (13) and (14) accounted for the fields in the aperture-bolus-air-muscle interfaces peculiar to the SMA, CSA or any other applicator set-up for treatment planning in electromagnetic hyperthermia.
- In Fig. 3, although the relative amplitudes of the CSA and SMA are virtually identical, their wave fronts are completely different. The CSA has a quasi plane wave front (varying by only $\sim 4°$ across the aperture) while the SMA has a wave front that varies in excess of 90° across its aperture. The CSA is a more efficient applicator [3]; it provides a higher penetration depth and a bigger effective field size (EFS) [5].

4. SIMULATED ENHANCEMENT RESULTS IN LUNG-LIKE LIQUID PHANTOM

The CSA has been used effectively for cancer therapy for several years. It has quasi-plane waves that result in deeper penetration at 450 MHz, compared to its contemporary applicators [3]. A lung-like liquid phantom was used as a homogeneous medium for SAR simulations at 450 MHz with conductivity $\sigma = 0.3\,\mathrm{S\ m^{-1}}$ and relative permittivity $\varepsilon_r = 35$. GBM simulations of SAR were performed for an

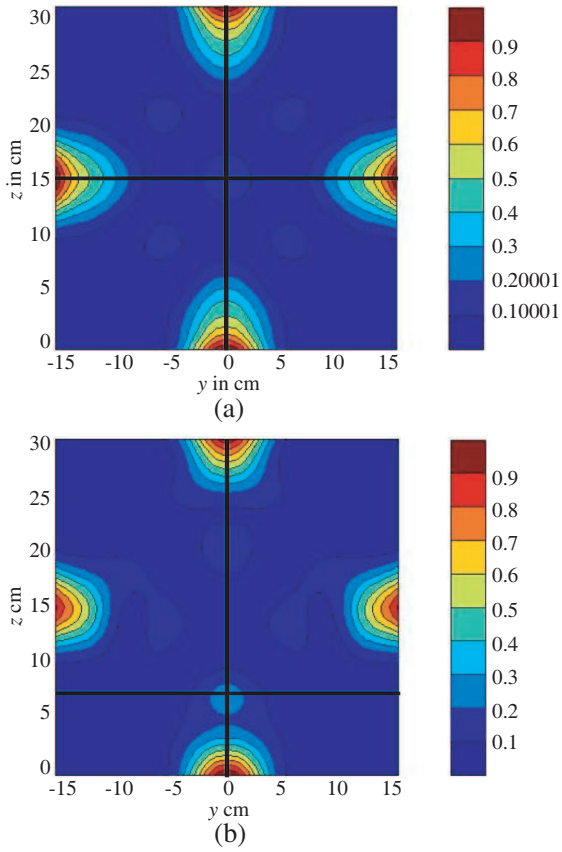

Figure 4. (a) 4-element SAR focus at center ($y = 0\,\mathrm{cm}$, $z = 15\,\mathrm{cm}$) of $30\,\mathrm{cm}^2$ of lung-like liquid phantom at 450 MHz ($\sigma = 0.3\,\mathrm{S\ m^{-1}}$ and $\varepsilon_r = 35$). (b) 4-element SAR focus off-center ($y = 0\,\mathrm{cm}$, $z = 7.5\,\mathrm{cm}$) of $30\,\mathrm{cm}^2$ of lung-like liquid phantom at 450 MHz ($\sigma = 0.3\,\mathrm{S\ m^{-1}}$ and $\varepsilon_r = 35$).

x-polarized electric field $E_x(y, z)$ by application of Equations (7)–(12) using MATLAB software. The simulated results for a variety of multi-element phased array configurations, and SAR focus or enhancement locations, relative to tumor targets (intersections of lines), are shown in Fig. 4 and Fig. 5.

The simulation results from 4-element and 8-element CSA-arrays for enhanced SAR at 450 MHz on various targets of a 30 cm^2 lung-like liquid phantom are shown in Fig. 4 and Fig. 5. It is clear from Fig. 4(a) through Fig. 5(b) that the SAR levels deposited at the prescribed targets (intersections of lines) are much higher for the 8-element CSA-arrays (70–80%) than for the 4-element CSA-arrays (20–30%). Theoretically, this indicates that for relatively deep hyperthermia a high number of elements must be used to achieve acceptable heating levels at tumor sites [2–5].

The 4-element and 8-element CSA array results for SAR

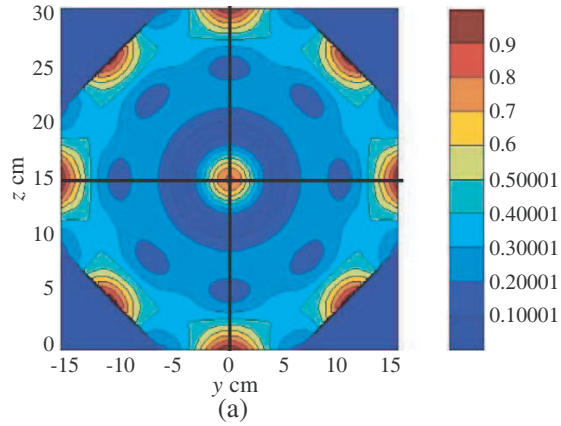

(a)

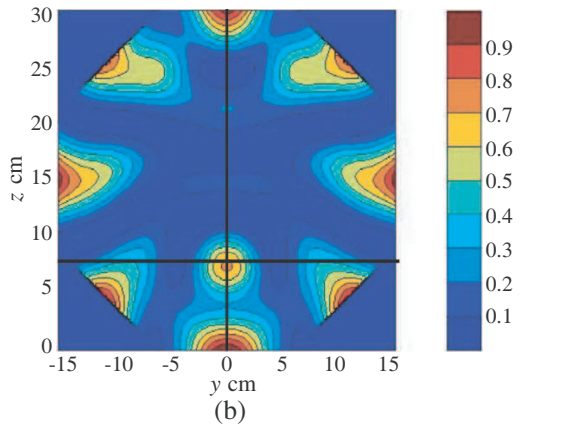

(b)

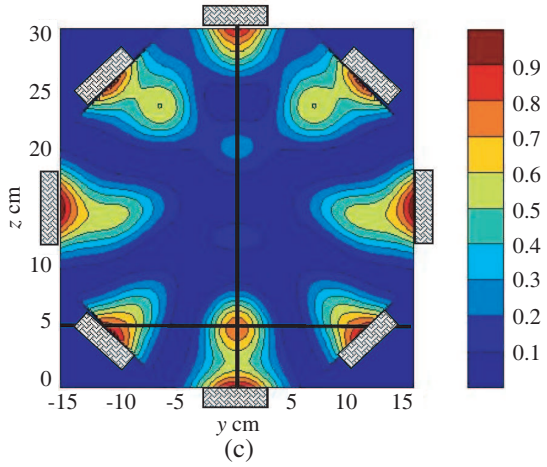

Figure 5. (a) 8-element SAR focus at center ($y = 0\,\text{cm}$, $z = 15\,\text{cm}$) of $30\,\text{cm}^2$ of lung-like liquid phantom at 450 MHz ($\sigma = 0.3\,\text{S m}^{-1}$ and $\varepsilon_r = 35$). (b) 8-element SAR focus off-center ($y = 0\,\text{cm}$, $z = 7.5\,\text{cm}$) of $30\,\text{cm}^2$ of lung-like liquid phantom at 450 MHz ($\sigma = 0.3\,\text{S m}^{-1}$ and $\varepsilon_r = 35$). (c) 8-element SAR focus off-center ($y = 0\,\text{cm}$, $z = 5\,\text{cm}$) of $30\,\text{cm}^2$ of lung-like liquid phantom at 450 MHz ($\sigma = 0.3\,\text{S m}^{-1}$ and $\varepsilon_r = 35$), with the 8 CSAs depicted.

enhancement simulations at the center of the lung-like liquid phantom in Fig. 4(a) and Fig. 5(a) are accurate (coincident with intersections of lines). This is because they are located within the paraxial region of each CSA element, and the phases of the CSA elements are identically set to focus at the respective centers of the phantom.

On the other hand, in Fig. 4(b), Fig. 5(b) and Fig. 5(c), the SAR enhancement simulations are accurate along the axial, z-directions (paraxial regions) only, but approximate (off intersections of lines) off the axial z-directions (non-paraxial regions). This is because the focal points or targets indicated in the Figures (intersections of axial, z-directed lines and transverse, y-directed lines) are coincident with the paraxial regions of 2 opposite CSA elements only in Fig. 4(b), Fig. 5(b) and Fig. 5(c). For the other elements, these focal points are located in non-paraxial regions, thus giving an approximate enhancement simulation of the SAR as far as the target is concerned. This is consistent with the GBM theory discussed in Section 2 and illustrated in Fig. 1.

5. CONCLUSION

As reported in [1–4] and referenced in [19, 20], the GBM includes data of measured field distributions in the aperture–bolus–air–phantom interfaces to avoid potential simulation errors. A lung-like liquid phantom was used in this study as it had previously provided experimental data that were replicated by the GBM, both for homogeneous and layered phantom-media of fat, muscle and lung [2, 4, 5], excluding simulation of SAR focus. This paper shows that GBM simulations of SAR focus in the paraxial region are accurate, but approximate in non-paraxial regions. Thus, the results can be used as a guide for treatment planning in electromagnetic hyperthermia. The orientation of phased array elements must be such that targets are located within the axial, z-directed, paraxial region defined by most of the multi-element applicator arrays. The simulated SAR enhancement results can be used to identify the target sites (intersection of axial, z-directed lines and transverse, y-directed lines). A minor corrective action can then be applied to the phase of each of the multi-element array of applicators (e.g., CSA) to optimize the SAR focus or enhancement on targets such as tumors.

ACKNOWLEDGMENT

This paper is dedicated to the late Dr. J. R. Wait, Emeritus Regents Professor of Electrical and Computer Engineering at the University of Arizona, Tucson. Approximately a year before he passed away, Dr. Wait sent the final of his annual research updates to the author, whom he had mentored at the University of Arizona (1983–1988). The letter included 13 copies of his journal publications in one year, with the following note: **"The tank is a bit low."** He continued, "A good journal paper would be to apply the focal theory from our work [2, 16, 17] to the Gaussian Beam Model." A recent review of the letter prompted the author to write this paper in memory of Professor J. R. Wait who could have been a Worthy Co-author of this paper.

REFERENCES

1. Andersen, J. B., "Electromagnetic power deposition: Inhomogeneous media, applicators and phased arrays," *Physics and Technology of Hyperthermia,* S. B. Field and C. Franconi (eds.), 159–188, Dordrecht, Martinus Nijhoff, The Netherlands, 1987.

2. Lumori, M. L. D., "Microwave power deposition in bounded and inhomogeneous lossy media," Ph.D. Dissertation, Department of Electrical and Computer Engineering, University of Arizona, Tucson, May 1988.
3. Lumori, M. L. D., "Experimentally based modeling of field sources for three-dimensional computation of SAR in electromagnetic hyperthermia and treatment planning," *IEEE Trans. Microwave Theory Tech.*, Vol. 48, 1522–1530, 2000.
4. Lumori, M. L. D., J. B. Anderson, M. K. Gopal, and T. C. Cetas, "Gaussian beam representation of aperture fields in layered, lossy media: Simulation and experiment," *IEEE Trans. Microwave Theory Tech.*, Vol. 38, 1623–1630, 1990.
5. Lumori, M. L. D., J. W. Hand, M. K. Gopal, and T. C. Cetas, "Use of Gaussian beam model in predicting SAR distributions from current sheet applicators," *Phys. Med. Biol.*, Vol. 35, 387–397, UK, 1990.
6. Gopal, M. K., J. W. Hand, M. L. D. Lumori, S. Alkhairi, K. D. Paulsen, and T. C. Cetas, "Current sheet applicator arrays for superficial hyperthermia of chestwall lesions," *Int. J. Hyperthermia*, Vol. 8, 227–240, 1992.
7. Prior, M. V., M. L. D. Lumori, J. W. Hand, G. Lamaitre, C. J. Schneider, and J. D. P. Van Dijk, "The use of current sheet applicator arrays for superficial hyperthermia: Incoherent versus coherent operation," *IEEE Trans. Biomed. Eng.*, Vol. 42, 694–698, 1995.
8. Deschamps, G. A., "Gaussian beam as a bundle of complex rays," *Electron. Lett.*, Vol. 7, No. 23, 684–685, Nov. 1971.
9. Deschamps, G. A., "Ray techniques in electromagnetic," *Proc. IEEE*, Vol. 60, 1022–1035, Sep. 1975.
10. Kogelnik, H., "On the propagation of Gaussian beams of light through lenslike media including those with loss or gain variation," *App. Opt.*, Vol. 4, No. 12, 1562–1569, 1965.
11. Kogelnik, H. and T. Li, "Laser beams and resonators," *Proc. IEEE*, Vol. 5, No. 10, 1550–1567, 1966.
12. Arnaud, J. A. and H. Kogelnik, "Gaussian light beams with general astigmatism," *Appl. Opt.*, Vol. 8, No. 8, 1687–1693, 1969.
13. Lovisolo, G. A., et al., "A multifrequency water-filled waveguide applicator: Thermal dosimetry in vivo," *IEEE Trans. Microwave Theory Tech.*, Vol. 32, No. 8, 893–896, 1982.
14. Johnson, R. H., "New type of compact electromagnetic applicator for hyperthermia in the treatment of cancer," *Electron. Lett.*,

Vol. 22, 591–593, 1986.

15. Johnson, R. H., A. W. Preece, J. W. Hand, and J. R. James, "A new type of lightweight low-frequency electromagnetic hyperthermia applicator," *IEEE Trans. Microwave Theory Tech.*, Vol. 35, 1317–1321, 1987.
16. Wait, J. R. and M. L. D. Lumori, "Focused heating in cylindrical targets, Part II," *IEEE Trans. Microwave Theory Tech.*, Vol. 34, 357–359, 1986.
17. Lumori, M. L. D., J. R. Wait, and T. C. Cetas, "Power deposition and focusing in a lossy cylinder by a concentric phased array," *Radio Science*, Vol. 24, 433–442, 1989.
18. Stogryn, A., "Equations for calculating the dielectric constant of saline water," *IEEE Trans. Microwave Theory Tech.*, Vol. 19, No. 8, 733–736, 1971.
19. Ebrahimi-Ganjeh, M. A. and A. R. Attari, "Study of water bolus effect on SAR penetration depth and effective field size for local hyperthermia," *Progress In Electromagnetics Research B*, Vol. 4, 273–283, 2008.
20. Gong, Y. and G. Wang, "Superficial tumor hyperthermia with flat left-handed metamaterial lens," *Progress In Electromagnetics Research*, PIER 98, 389–405, 2009.